

CFD SIMULATION OF BLADE LOAD DISTRIBUTION CONTROL AS ACTIVE CENTRIFUGAL COMPRESSOR SURGE SUPPRESSION

Károly Beneda

Turbomachines necessitates up-to-date methods to ensure economical and safe operation at the same time with the widest possible range that makes novel ideas inevitable to handle classical problems. The most dangerous instability in compression systems is surge that has to be suppressed before its onset to avoid structural damages or other different adverse consequences in the system. As surge occurs at low delivered mass flow rates the conventional widely spread surge control is based on bypassing or recycling the unnecessary airflow. This method is used on a large number of gas turbines and provides a robust control on suppressing compressor surge while its efficiency loss is significant. The aim of this paper is to show the results of CFD simulations of an active surge suppression concept using flow injection at a mid-span location rather than at the inlet. This injection leads to a different blade load distribution along its chord resulting in a possible effect of suppress instabilities. Its advantage over concurrent methods is that it can be based on up-to-date MEMS technology leading to moderate losses but comparable stability enhancement. Previously the one-dimensional mathematical model of the concept has been established, but it is inevitable – as a virtual prototyping – to carry out detailed numerical simulation of the device. The paper shows the results of this CFD simulation.

K e y w o r d s: compressor surge, active surge suppression, blade load distribution control, MEMS

1 INTRODUCTION

Centrifugal compressors are widely used in the industry and transportation, including the probably most safety critical application in aircraft power plants. The off-design behaviour, when throttling the mass flow rate to lower regions, includes severe instabilities that restrict the operational area. The most dangerous phenomenon is surge, regarding that it affects the operation of the whole system, and contains high energy that can easily damage system components.

Pure surge in compressors (whether axial or centrifugal) manifests in one-dimensional mass flow and pressure oscillation that depends not only on the operation of the compressor, but also is a function of downstream components of the system. In contrast to this, rotating stall is a consequence of compressor-related anomalies [5]. Based on the extents of the oscillation, one can differentiate the following species of surge [7]: *mild surge* that causes moderate fluctuations in annulus averaged mass flow rate but is incapable to excite other instabilities; *classic surge* increases angle of attack during oscillations beyond the stall limit but does not leads to backflow; *deep surge* is the most severe form that covers a complete reversal of the flow.

Severe consequences range from increase of mechanical loads on unique components to problems related to the complete system like combustion chamber flameout, when using the given compressor in a gas turbine. It is obvious that the consequences of surge necessitate solutions that can provide avoidance or suppression of surge.

2 DESCRIPTION OF BLADE LOAD DISTRIBUTION CONTROL (BLDC)

2.1 Original concept of BLDC

An interesting research in the late 1970's showed the evidence that the merging stalled regions of inducer and impeller flow passage can be a possible cause for

growing global instability [8]. Modification of the blade load distribution results in stable operation at lower mass flow rates. The concept was developed originally as a fixed geometry modification of common centrifugal blade, as seen on Figure 1. Due to its significant increase in rotational inertia it could not spread widely.

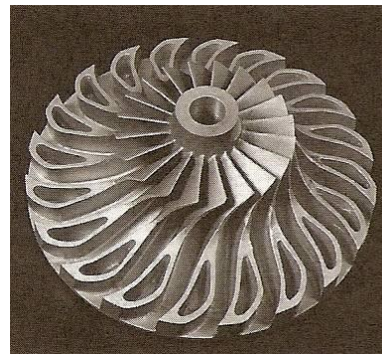


Figure 1 Modified impeller for control of separation [13]

In the recent decades the micro-electro-mechanical systems (MEMS) emerged. These devices can be used for solving problems, which were difficult or impossible when relying on conventional methods. The aim of this paper is to investigate such possibilities that are similar to the original concept but can provide control of blade load distribution in order to reach active surge suppression capabilities.

2.2 Active BLDC Using Flow Injection

There is a widely known possibility of flow pattern modification within the impeller blade passages using flow injection. Great majority of the investigations have aimed at compressor inlet injection (e.g. [11], [12]) energizing the near-stall blade tip airflow resulting in enhanced stability [17].

In contrast to inlet injection the mid-span inflow, which is the topic of the present paper, modulates dynamically the effective cross-sectional area leading to flow stabilization. The flow injected BLDC is similar to the problem involved in air-fuel mixing in combustion

chambers (e.g. [10], and [14]), film cooling of gas turbine components [15], and several basic jet in a cross-flow investigation of these conditions (e.g. [6], [16], [18]). In order to establish the basis for the theory of BLDC, the results of these general researches have to be utilized. The concept of a jet in a cross-flow is presented on Fig. 2.

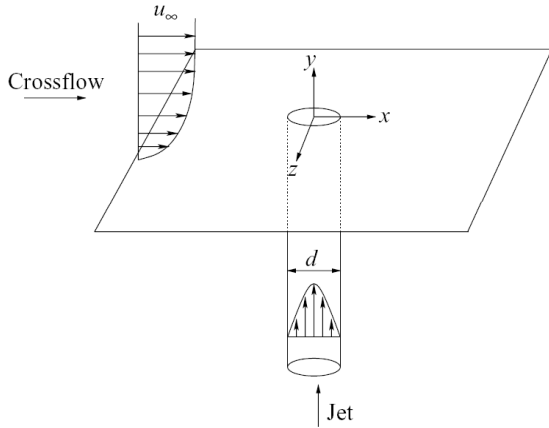


Figure 2 Schematic of jet in cross flow problem presented in the BLDC concept (adapted from [16])

The injection would be more efficient if it could be realized through the suction surface of the impeller blade, but due to the thin material it leads to strength issues. Therefore, the present research is based on the compressor hub as a possible source of injected flow.

2.3 Mathematical model of BLDC

The author has established a one-dimensional mathematical model for investigation of effects of various surge suppression methods, including BLDC and variable inducer shroud bleed. This computation method handles the centrifugal compressor as a logically separated dual device (inducer and impeller) connected in series. Therefore the Split Compression Model (SCM) can be considered as an outgrowth of the Two-Elements-In-Series (TEIS) model described in [13]. The computation is based on conventional one-dimensional methods completed with the conservation laws between the inducer and impeller, which are detailed in [1] and [3]. The logical setup of the model can be seen on Fig. 3, while the important aero-thermodynamic stations are illustrated on Fig. 4.

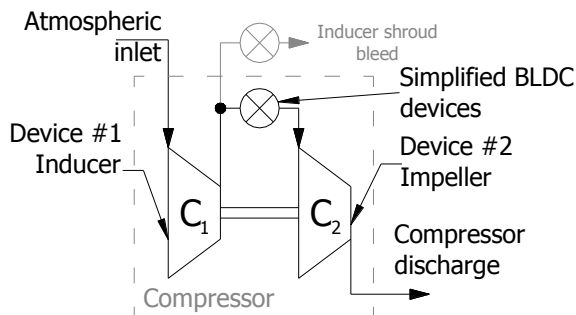


Figure 3 Schematic of Split Compression Model

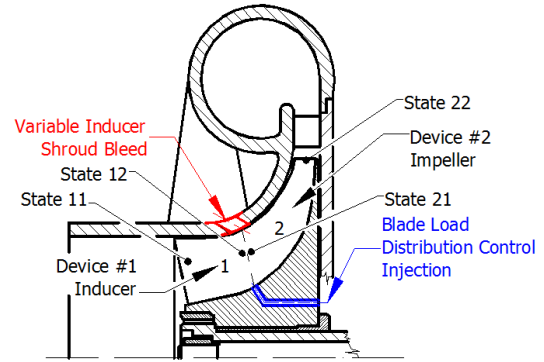


Figure 4 Aero-thermodynamic stations of SCM

The governing equations of the SCM can be written for a single unit (inducer or impeller) as follows:

$$\Delta h_{i,id}^* = u_{i2} \cdot c_{i2,u} - u_{i1} \cdot c_{i1,u} = c_p \cdot \Delta T_{i,id}^* \quad (1)$$

Equation (1) describes the conservation of energy throughout the i^{th} unit assuming ideal conditions. Here $\Delta h_{i,id}^*$ is the ideal change in stagnation enthalpy, u is the peripheral velocity, c is the absolute velocity of the flow, $\Delta T_{i,id}^*$ stands for ideal stagnation temperature rise.

It is important to include the calculation of the tangential component of the absolute velocity at the exit of the given unit. This is commonly established using the formula:

$$c_{i2,u} = \sigma_i \cdot u_{i2} \quad (2)$$

In Eq. (2), σ_i , the slip factor of the i^{th} unit can be calculated using e.g. the Stanitz-formula for slip factor in a centrifugal compressor, amending the original expression with a specific exponent, which realizes the criterion that the slip factor in the inducer equals to unity:

$$\sigma_i = \left(1 - \frac{2}{z}\right)^{(i-1)} \quad (3)$$

The real case with the most important losses can be modelled as follows:

$$\Delta h_i^* = \Delta h_{i,id}^* + \Delta h_{i,fric}^* + \Delta h_{i,inc}^* \quad (4)$$

$$\Delta h_{i,fric}^* = K_c \cdot \dot{m}^2 \quad (5)$$

$$\Delta h_{i,inc}^* = \frac{1}{2} \cdot \left(u_{i1} - \frac{\cot \beta_{1g} \cdot \dot{m}}{\rho_{i1} \cdot A_{i1}} \right)^2 \quad (6)$$

Based on [9] the friction loss in Eq. (5) can be expressed as the second exponent of mass flow rate along with its coefficient K_c . Equation (6) defines incidence loss whose deduction can be found in [9].

The efficiency of the given unit can be expressed as the ratio of ideal and real stagnation enthalpy rises:

$$\eta_i = \frac{\Delta h_{i,id}^*}{\Delta h_i^*} = \frac{\Delta h_{i,id}^*}{\Delta h_{i,id}^* + \Delta h_{i,fric}^* + \Delta h_{i,inc}^*} \quad (7)$$

From the expression of efficiency one can determine the outlet total pressure of the unit using the following formula:

$$p_{i2}^* = p_{i1}^* \cdot \left(1 + \frac{\eta_i \cdot \Delta h_{i,id}^*}{c_p \cdot T_{i1}^*} \right)^{\frac{\kappa}{\kappa-1}} \quad (8)$$

Possessing the discharge pressure, it is also important to verify whether the required pressure for maintaining the necessary inflow is below the discharge pressure. This is inevitable for using the compressor as the source for flow injection. The determination of relationship between required pressure and injection rate is the goal of the present research.

The forthcoming considerations concern the continuity between the two parts, where the basic flow can be modified two ways. One possibility is the Variable Inducer Shroud Bleed (VISB) that is detailed in [2] and [3], which manifests in a smaller impeller mass flow compared to the flow through the inducer. The other device is the BLDC that supplies additional flow into the domain having dual effect on the base flow:

1. the mass flow is increased by the amount of injected flow
2. the base flow is shifting towards the shroud that results in a higher u_{i2} (inducer outlet peripheral speed).
- 3.

The above mentioned assumptions can take the form of the following equations:

$$\dot{m}_{21} = \dot{m}_{i2} - \Delta \dot{m}_{VISB} + \Delta \dot{m}_{BLDC} \quad (9)$$

$$u_{i2} = [r_{i2,nom} + \Delta r_{i2}(\chi)] \cdot \omega_{(i)} \quad (10)$$

In Eq. (9) and (10), both VISB and BLDC can be considered as orifices with the given expression of mass flow shown in Eq. (11) and (12). The shifting effect is taken into account with the help of a Δr_{i2} change in inducer outlet mean radius, which is an appropriate function of the relative BLDC injection rate χ . The goal of the numerical simulations is to determine the relationship between these parameters.

$$\Delta \dot{m}_{VISB} = \gamma \cdot A_{VISB} \cdot \alpha_{VISB} \cdot \sqrt{2 \cdot \rho_{i2} \cdot (p_{i2} - p_0)} \quad (11)$$

$$\Delta \dot{m}_{BLDC} = \chi \cdot A_{BLDC} \cdot \alpha_{BLDC} \cdot \sqrt{2 \cdot \rho_{BLDC} \cdot (p_{BLDC} - p_{i2})} \quad (12)$$

In Equations (11) and (12) γ is the relative opening of the VISB, A is the surface of the respective

device, α is the coefficient of contraction; p_{i2} , p_0 and p_{BLDC} are the static pressures in the inducer outlet, ambient and BLDC input, respectively; ρ_{i2} designates inducer outlet density, ρ_{BLDC} stands for density of injected air.

2.4 Mathematical model of flow injection

The most important effect of the BLDC injection is the reduction of effective flow area and shifting to a higher radius inside the blade passage. These parameters have been inspected in the evaluation and both of them can be obtained from the jet trajectory. An important assumption is that the BLDC injection creates a nearly full cover over the impeller hub, similar to the film cooling of turbine blades [15]. The relationship between dimensionless streamwise location x/d and intrusion height y/d can be described as in Eq. (13) (from [6], refer to Fig. 2). The values of symbols a , b , and c can be obtained experimentally (refer to their respective limits shown in Eq. (14)), d is the jet diameter, while J stands for the momentum flux ratio of the jet and the cross flow, whose definition is shown in Eq. (15), with the help of ρ density and v velocity of the two flows [6].

$$\frac{y}{d} = a \cdot J^b \cdot \left(\frac{x}{d} \right)^c \quad (13)$$

For the factors in Eq. (13), the following relations must be achieved (after [6]):

$$\begin{aligned} 0.7 &\leq a \leq 1.3 \\ 0.36 &\leq b \leq 0.52 \\ 0.28 &\leq c \leq 0.4 \end{aligned} \quad (14)$$

$$J = \frac{\rho_{jet} \cdot v_{jet}^2}{\rho_{cf} \cdot v_{cf}^2} \quad (15)$$

It is important to note, that if the density of injected flow and the cross flow are approximately equal, the momentum flux ratio can be omitted and the velocity ratio can be used instead (Eq. (16), [6]). It is the case with small pressure ratio compressors, but the model incorporates the full momentum flux ratio in order to be able to compute higher pressure ratios also in the future.

$$R = \frac{v_{jet}}{v_{cf}} \quad (16)$$

If the jet is carrying a different phase (i.e. liquid is injected), the Weber number has also a high importance [10]. Since this is a similarity value describing the ratio of the inertial force to the tension force acting on a fluid element, therefore it is assumed to be negligible and is not used in this research.

3 INVESTIGATIONS USING COMPUTATIONAL FLUID DYNAMICS

The purpose of computational fluid dynamics (CFD) is to model physically-mathematically various fluid flows with the help of computers where, for any reason, the given investigation could not be realized or it would raise difficulties. Computers only execute user-given commands; therefore, they naturally cannot verify by their own whether the results are real or not. Thus, the validation part of the process is also inevitable.

CFD simulations have common base principle, namely, the conservation laws of mass, impulse and energy. These equations have to be written in their nonlinear differential form that, except for the simplest cases (e.g. stationary flow in a duct), cannot be solved directly. Due to the difficulty of analytic solution the numerical approach is necessary that includes discretization of the equation system and the flow domain also. That means the differential equations are converted to difference equations, where the differences are small enough, and they are solved in the selected points of the fluid domain.

The performance of personal computers went through a significant rise in the recent years, which lead to an emerging accessibility of CFD software for smaller companies and educational entities. At the author's Department the ANSYS multi-physics commercial code is available that is also used in the present investigation. The research included a simplified model which simulated a single blade channel with BLDC devices.

3.1 Simplified model of centrifugal compressor with BLDC

The simplified model was used to determine the effect of the injected flow in the given environment in order to reduce the time required for the simulation. It had the role to get the answer whether the compressor outlet pressure can create significant deflection of the original flow if used for injection. Its setup can be seen on Fig. 5, where the three different domains (stationary inlet and outlet, and rotating blade passage) are illustrated and one can identify the major boundary conditions also.

The inlet is light blue, and there are two sides with symmetric boundary condition highlighted with magenta, because the inlet domain is assumed to carry axisymmetric flow. The outer surface of the blade passage is a stationary shroud, which is commonly modelled as a counter-rotating wall when the relative movement of this region is compared to the impeller itself. The counter-rotating wall is coloured green and it has an important offset from the blade tip that can be investigated on the detail of Fig. 5. Moving into the stationary frame, within the outlet domain one can identify the discharge cross-section marked with red. In contrast to the inlet, in this region there is a high tangential velocity component due to the effect of the impeller, so the flow cannot be

considered axis-symmetric. Therefore, on the two sides illuminated with amber, a rotational periodicity was required. On the other hand, rotational periodicity is not a simple boundary condition but rather an interface between the two surfaces that were created during the extraction of a single blade passage from the whole compressor unit.

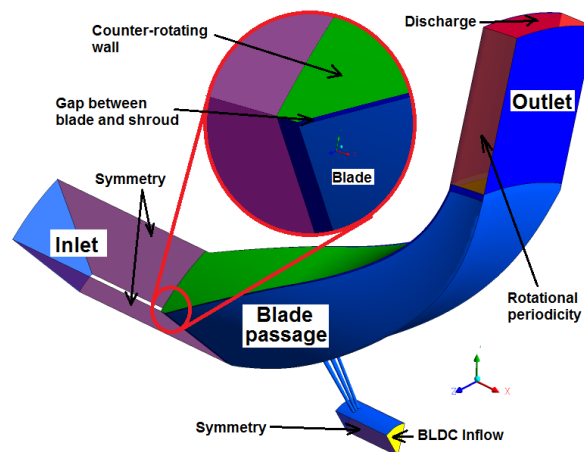


Figure 5 Setup of simplified model with boundary conditions

The model was meshed using patch conforming tetrahedral elements in six different cases, in which the global number of nodes ranged from approximately 250.000 up to nearly 3.0 million. It was a very important part of the investigation to focus on the dependence of simulated values on the mesh resolution. On rigid wall surfaces there was inflation in order to enable efficient boundary layer calculation. Details of the grid can be inspected on Fig. 6, where the close vicinity of the blade tip leading edge (coloured yellow) is visible. The mesh resolution has been locally increased in the gap between blade tip and shroud in order to be able to simulate the losses arising here. Figure 6 also offers an insight into the blade passage using a section plane just downstream of the blade leading edge.

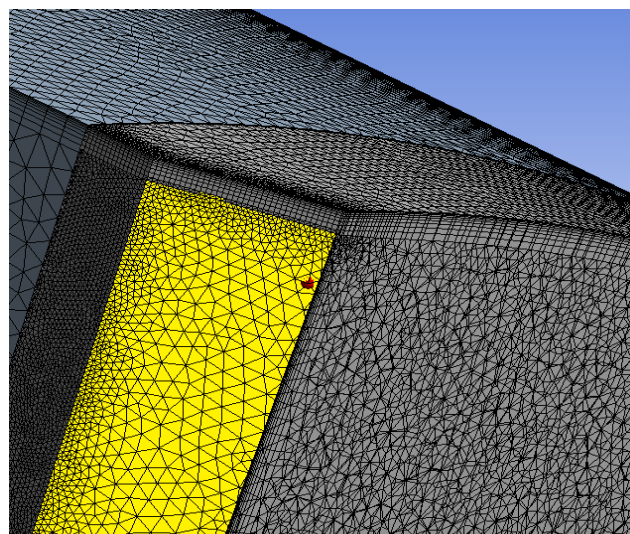


Figure 6 Details of mesh at the blade tip leading edge

After the grid generation, the setup has to clarify boundary conditions and other important parameters. At the outlet and BLDC injection the mass flow rates were determined, while the inlet had a uniform total pressure of zero value relative to the ambient. The rotating domain of blade passage had a rotation speed of 17803 rpm that corresponds to the nominal speed of the compressor involved in the present research.

Following the mesh independency investigation, several injection rates have been investigated in the range of 0 and 2.5% of the outlet flow. between zero and unity every quarter percents was involved in the simulations, above one all half percents was examined, so a total of seven cases were involved in the present investigation.

4 EVALUATION OF RESULTS

4.1 Mesh accuracy

After the solution phase has been completed, an important verification is to be carried out. The dimensionless wall distance has to match the relationship shown in Eq. (17). This is indispensable to consider a solution as a mirror of reality. The definition of y^+ is found in Eq. (18), where u_τ is the friction velocity and ν is the kinematic viscosity, and y is the physical distance measured from the wall.

$$y^+ < 200 \tag{17}$$

$$y^+ = \frac{y \cdot u_\tau}{\nu} \tag{18}$$

The above mentioned meshes were enough to provide the required values, as it can be evaluated on Fig. 7 and Table 1.

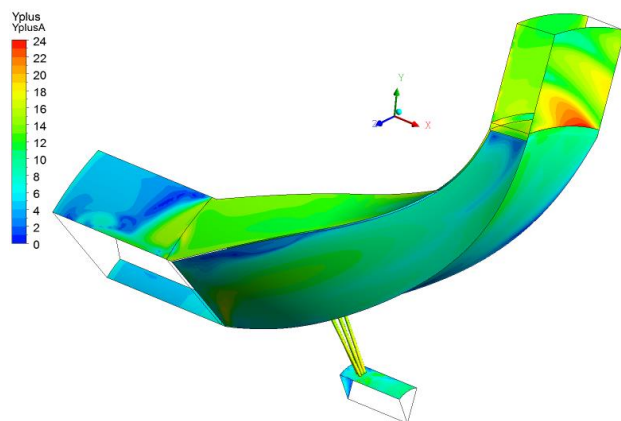


Figure 7 y^+ values of the mesh of 1,75 million nodes

TABLE 1. Maximal y^+ and total pressure at BLDC injection as a comparison of different mesh resolutions

Number of nodes	y^+_{max} (-)	$p_{T,BLDC}$ (Pa)
397069	34,31	9825,25
599435	50,89	9848,77
964423	29,23	9740,46
1259877	23,97	9949,92
1760096	24,06	9969,19
2990956	22,56	9910,79

4.2 Evaluating jet trajectory

As the possibility for validation through own physical realization of the system is not provided, the evaluation of the results have been carried out using a significant number of articles in the field of jet in a cross flow, comparison with available solutions of similar problems can be used.

In order to obtain the necessary basis for comparison between trajectories of the given computation and others, first of all, the velocities and densities of the jet and the cross-flow have to be calculated. For this purpose, the ANSYS Function Calculator was used, which is a built-in application in the CFD post-processing environment.

The compressor involved in the investigation creates a peak total-to-total pressure ratio at nominal speed of only $\pi_c^* \approx 1.25$ ([2]), therefore the density of the jet and the crossing basic flow does not differ significantly, i.e. both were in the range of

$$1,21 \frac{kg}{m^3} \leq \rho_{jet}, \rho_{cf} \leq 1,23 \tag{19}$$

During the simulations it was also important that the cross flow velocity inside the blade passage remained almost the same during all cases, therefore it is assumed a constant value that corresponds to a near surge situation in the given compressor.

$$v_{cf} = 47,15 m/s \tag{20}$$

For easier reading of the following figures, they represent the maximum of injection rate as it comprises the highest possible deflection value. The streamlines are shown on Fig. 8, and the correlation of jet trajectory is visualized on Fig. 9 along with a comparison to the model described in [6].

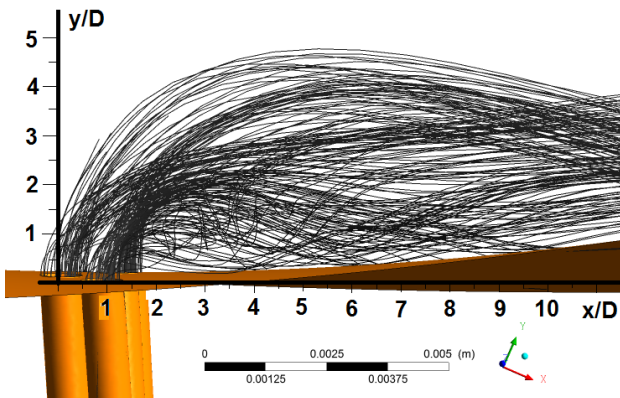


Figure 8 Streamlines entering the base flow with relative coordinates displayed [4]

Based on Eq. (13), the correlation between streamwise dimensionless length x/d (where d is the diameter of the jet orifice) and dimensionless intrusion height y/d was established using the guidelines found in [6].

The coefficients of Eq. (13) have been chosen to their respective limits; which has led to a slightly higher intrusion height (solid red line on Fig. 9) compared to the simulation results.

The latter are shown with discrete points (light blue diamonds on Fig. 9) and if one chooses coefficients slightly beyond the limits, a satisfactory fit can be achieved (dashed blue line on Fig. 9). The difference between simulated and predicted values reach the 5% limit at approximately $x/d = 4$ while the maximum difference is about 12.0%.

Taking into account the special conditions of the given problem, it is a realistic assumption that the comparably sharp bend in a centrifugal compressor impeller can result in a reduced intrusion capability of the jet having the same velocity or momentum flux ratio compared to two dimensional arrangements that can be found in the referenced literature.

The correlation, that is found between dimensionless streamwise coordinate x/d and dimensionless intrusion height y/d can be described as follows:

$$\frac{y}{d} = 0,7 \cdot J^{0,55} \cdot \left(\frac{x}{d}\right)^{0,2} \quad (21)$$

When compared to Eq. (14), the values of coefficients b and c are slightly exceeding the experimental limits from other sources. The reason was emphasized and explained above, and therefore the obtained results are considered applicable.

TABLE 2. Comparison of momentum flux ratios of various injection rates

Injection rate (% of nominal flow)	Jet velocity (m/s)	Momentum flux ratio (-)
0,25	13,59	0,083
0,50	26,35	0,312
0,75	35,65	0,572
1,00	47,65	1,021
1,50	72,61	2,372
2,00	97,94	4,315
2,50	121,73	6,665

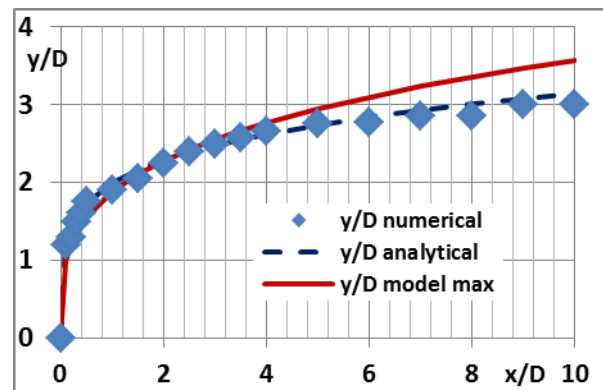


Figure 9 Correlation between dimensionless axial distance and intrusion height

A total of seven cases were investigated with increasing injected flow ratio, as noted above. Table 2 summarizes the momentum flux values that were used for validation. It is evident that due to the very small difference in jet and cross flow densities (characterized in Eq. 18) these figures are relatively small.

4.3 Consequences of the mathematical model

The simulations resulted in two very important values, the maximum intrusion height achieved by a given injection rate and the required pressure difference to drive the injection. These can be evaluated on Fig. 10 which shows the dependence of the two above mentioned variables as a function of injection rate the latter shows the streamlines of the flow pattern. It is interesting that the high ascent rate of intrusion height at the beginning of the injection reduces as injection reaches significant values. It is also important to note that the compressor at the examined revolution speed creates approximately 23kPa pressure rise ([2]) that is hardly above the pressure that is required to drive the injection at the upper limit of approximately 3%. The last value with 2.8% injection rate is adapted from the entire compressor model simulations ([4]).

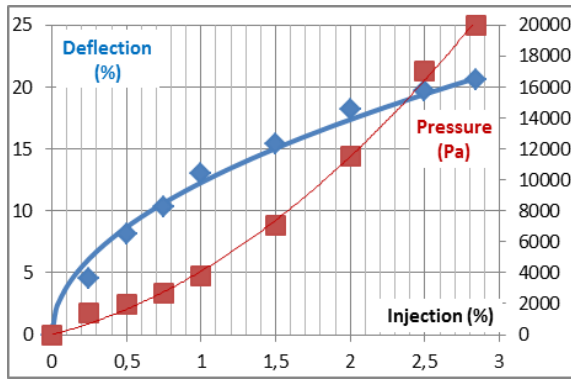


Figure 10 Dependence of intrusion height and required pressure on the relative mass flow rate of injection

The object of the present investigation was to obtain data about the operation of the flow injection in order to incorporate the results in the Split Compression Model. The original assumption, that the BLDC can be considered as a simple orifice, had to be refined.

As a consequence of the results, the Euler equation in the Split Compression Method has to be calculated using Eq. (10) describing the shifting effect of the injected flow. Referring to Fig. 10, the simulations have reached their goal; it is possible to determine an approximate relationship between the injection rate and the resulting deflection. Taking into account the shape of the blue curve on Fig. 10, an assumed square root function is established:

$$\Delta r_{12}(\chi) = K_{\chi} \cdot \sqrt{\chi} \cdot (r_{12,tip} - r_{12,hub}) \quad (22)$$

where K_{χ} is a constant, $r_{12,tip}$ and $r_{12,hub}$ are the tip and hub radii in the inducer outlet cross-section, respectively. If χ is substituted as a percentage of the base flow, K_{χ} holds a value of 1.23.

The final verification of the possibility of a given injection rate is also important when the BLDC source is the compressor outlet. In such a case, the corresponding correlation between injection rate and required pressure is the following:

$$\Delta p_{BLDC}(\chi) = [p_{BLDC} - p_{12}](\chi) = K_{p2} \cdot \chi^2 + K_{p1} \cdot \chi \quad (23)$$

As it can be evaluated on Fig. 10, Δp_{BLDC} has a second order polynomial relation to the injection rate, with a constraint of zero injection requires zero pressure difference.

5 CONCLUSIONS

It has been shown in the previous chapters with the help of the simplified model, that the flow injection for active blade load distribution control is likely to be applicable. The method results in such a flow field modification, which leads to the presence of a converging

section within the blade passage that is able to prevent surge. The investigation showed that the compressor discharge pressure is able to create significant injection rates making it a possible source of this system.

In addition, the flow injected from the hub of the impeller results in a shifted base flow towards the shroud region. In a conventional one-dimensional approach it increases the mean diameter of the effective flow passage leading to a rising Euler-head within the inducer while decreasing the head of the impeller. This change in blade load distribution can be a source of flow stabilization as the original survey [8] has shown.

Nevertheless, the results of this investigation form only a small part of the whole research, which is focusing on the applicability of MEMS devices in the studied surge suppression methods. Therefore, a throughout survey about the dynamical behaviour of the possible devices are also of high importance along with the control theory of the complete system including these elements.

BIBLIOGRAPHY

- [1] BENEDA, K. – NAGY, A.: Investigation of Compressor Surge Control Using Nonlinear Mathematical Model and Realizing by MEMS Technology. In: Seventh International Conference on Mathematical Problems in Engineering, Aerospace and Sciences. Cambridge Scientific Publishers, Cottenham, 2009, pp. 732-741.
- [2] BENEDA, K.: Experimental Investigation of Centrifugal Compressor Surge Protection Using Variable Inducer Shroud Bleed. In: MOSATT 2011 Modern Safety Technologies in Transportation, Proceedings of the International Scientific Conference Vol. 4 (2011), pp. 18-23.
- [3] BENEDA, K.: Preliminary Results of Active Centrifugal Compressor Surge Control Using Variable Inducer Shroud Bleed. Periodica Polytechnica Transportation Engineering Vol. 39/2 (2011), pp. 49-54, DOI: 10.3311/pp.tr.2011-2.01
- [4] BENEDA, K.: Numerical simulation of MEMS-based blade load distribution control in centrifugal compressor surge suppression. In: AIP Conference Proceedings, Vol. 1493 (2012), pp. 116-123, DOI: 10.1063/1.4765479
- [5] DAY, I. J., GREITZER, E. M., and CUMPSTY, N. A.: Prediction of Compressor Performance in Rotating Stall. ASME Journal of Engineering for Power, Vol. 100 (1978), pp. 1-12.
- [6] DEMUREN, A. O.: Modeling Jet in a Cross Flow. NASA Langley Research Center, Hampton, 1994.
- [7] FLOWCS WILLIAMS, J. E., HARPER, M. E. L., and ALLWRIGHT, D. J.: Active stabilization of compressor instability and surge in a working engine. ASME Journal of Turbomachines, Vol. 115 (1993), pp. 68-75.
- [8] FLYNN, P.F. - WEBER H.G.: Design and test of an extremely wide flow range compressor, ASME Paper 79-GT-80 (1979).
- [9] GRAVDAHL, J. T., – EGELAND, O.: Centrifugal Compressor Speed and Surge Control. IEEE Transactions on Control Systems Technology, Vol. 7 (1999), pp. 567-579.
- [10] HERMANN, M., ARIENTI, M., and SOTERIOU, M.: The Impact of Density Ratio on the Liquid Core Dynamics

- of a Turbulent Liquid Jet Injected Into a Crossflow. *Journal of Engineering for Gas Turbines and Power*, Vol. 133 (2011), DOI: 10.1115/1.4002273.
- [11] HILLER, S. J., MATZGELLER, R., and HORN, W.: Stability Enhancement of a Multistage Compressor by Air Injection. *Journal of Turbomachinery*, Vol. 133 (2011), DOI 10.1115/1.4001228.
- [12] HORN, W., SCHMIDT K. J., and STAUDACHER, S.: Effects of Compressor Tip Injection on Aircraft Engine Performance and Stability. *Journal of Turbomachinery*, Vol. 131 (2009), DOI: 10.1115/1.2988159.
- [13] JAPIKSE, D.: *Centrifugal Compressor Design and Performance*. Concepts ETI, Wilder (USA), 1996. ISBN 0-933283-03-2.
- [14] KRAUTKREMER, B. H., BLOMEYER, M. M., and HENNECKE, D. K.: Optical Measurements of Jet-Mixing in a Swirling Crossflow of a Combustion Chamber. In: *RTO AVT Symposium on Gas Turbine Engine Combustion, Emissions and Alternative Fuels*, RTO MP-14, 1998, pp. 42.1-42.11.
- [15] KUNZE, M., VOGELER, K., BROWN, G., PRAKASH, C., and LANDIS, K.: Aerodynamic and Endwall Film-Cooling Investigations of a Gas Turbine Nozzle Guide Vane Applying Temperature-Sensitive Paint. *Journal of Turbomachinery*, Vol. 133 (2011), DOI: 10.1115/1.4003426.
- [16] MUPPIDI, S. – MAHESH, K.: Direct Numerical Simulation of Turbulent Jets in Crossflow. In: *43rd AIAA Aerospace Sciences Meeting and Exhibit, 2005*, pp. 1-15. http://www.aem.umn.edu/~mahesh/publpdf/conference/su-man_aiaa_05.pdf
- [17] STEIN, A., NIAZI, S., and SANKAR L. N.: Computational Analysis of Centrifugal Compressor Surge Control Using Air Injection. *Journal of Aircraft* Vol. 38 (2001), pp. 513-521.
- [18] SUNDARARAJ, S., – SELLADURAI, V.: The Effects of Arbitrary Injection Angle and Flow Conditions on Venturi-Jet Mixer. *Thermal Science*, Vol. 16 (2012), pp. 207-221. DOI: 102298/TSCI101023059S

AUTHORS' ADDRESS

Beneda Károly, professor's assistant
Budapest University of Technology and Economics
Department of Aircraft and Ships
e-mail: beneda@rht.bme.hu